Macromolecules

Article

pubs.acs.org/Macromolecules

Ionic Conduction and Dielectric Response of Poly(imidazolium acrylate) Ionomers

U Hyeok Choi,[†] Minjae Lee,[‡] Sharon Wang,[§] Wenjuan Liu,[†] Karen I. Winey,[§] Harry W. Gibson,[‡] and Ralph H. Colby*,[†]

[†]Department of Materials Science and Engineering, Pennsylvania State University, University Park, Pennsylvania 16802, United States

[‡]Department of Chemistry, Virginia Polytechnic Institute and State University, Blacksburg, Virginia 24061, United States

[§]Department of Materials Science and Engineering, University of Pennsylvania, Philadelphia, Pennsylvania 19104, United States

Supporting Information

ABSTRACT: We use X-ray scattering to investigate morphology and dielectric spectroscopy to study ionic conduction and dielectric response of imidazolium-based single-ion conductors with two different counterions [hexafluorophosphate (PF_6^-) or bis(trifluoromethanesulfonyl)imide ($F_3CSO_2NSO_2CF_3^-$ = Tf_2N^-)] with different imidazolium pendant structures, particularly tail length (*n*-butyl vs *n*-dodecyl). A physical model of electrode polarization is used to separate ionic conductivity of the ionomers into number density of conducting ions and their mobility. Tf_2N^- counterions display higher ionic conductivity and mobility than PF_6^- counterions, as anticipated by *ab initio* calculations. Ion mobility is coupled to polymer segmental motion, as these are observed to share the same Vogel temperature. Ionomers with the *n*-butyl tail impart much larger static dielectric constant than those with the *n*-dodecyl tail. From the analysis of the static dielectric constant using Onsager theory, there is more ionic aggregation in ionomers with the *n*-dodecyl tails than in those with the *n*-butyl tails, consistent with X-ray scattering, which shows a much stronger ionic aggregate peak for the ionomers with dodecyl tails on their imidazolium side chains.

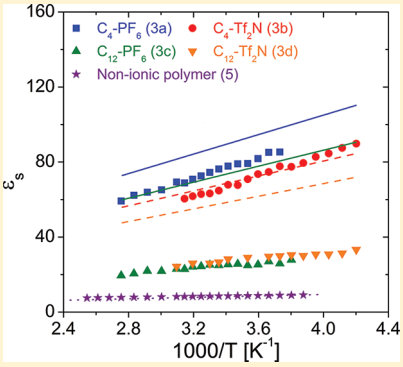

1. INTRODUCTION

Ionic conduction in ion-containing polymers is of considerable interest from both fundamental and applied points of view. Recently, ionic liquids, which are composed entirely of large cations and anions with weak interactions (310 kJ/mol for 1-butyl-3-methylimidazolium cation with Tf_2N^- counterion at 0 K in vacuum),[1] have attracted significant interest due to their unique physical properties such as high thermal and chemical stability, negligible vapor pressure, broad electrochemical window (many are stable up to 5 V), and high ionic conductivity.[2−9] In particular, a number of groups have described imidazolium salts in which the geometric packing constraints of the planar imidazolium ring, its dangling alkyl groups, and the delocalization of the charge over the N−C−N moiety in the ring together reduce ion−ion interactions.[6,9−11] These remarkable characteristics make it possible for ionic liquids to be used as novel and safe electrolytes for advanced devices such as electrochemical membranes for capacitors, lithium batteries, fuel cells, and electromechanical transduction devices for actuators and sensors.[12−21] There is a wide chemical composition range of ionic liquids, achieved by pairing various organic cations with numerous anions that allows for fine control of their physicochemical properties.

Moreover, imidazoliums and other organic ionic liquid cations can be synthesized with vinyl groups so that they can be easily incorporated into polymers, so-called polymerized ionic liquids, which carry an ionic liquid species in each of the repeating units.[22−34] The major advantages of using the polymeric forms of ionic liquids are the enhanced stability and improved mechanical durability resulting from polymerization and the simplification that only the counterions are able to move large distances rapidly, making polymerized ionic liquids single-ion conductors. It is of great interest to understand the general physical picture of structure−property relations in polymerized ionic liquids. In this paper we focus on the effects of varying the tail length of the pendant imidazolium side chains and of two different popular anions as counterions.

Computer simulations have been used to investigate the influence of different counterions and cation chain lengths in imidazolium ionic liquids[35−39] that are not polymeric. As tail length increases, locally heterogeneous environments emerge, consisting of polar (anion/cation pairs) and nonpolar (tail) regions. Such a morphology has been suggested to affect viscosity, diffusion, and ionic conductivity. The polar regions form a variety of ionic structures, consisting of ion pairs and aggregates formed by dipolar interactions between pairs.[40]

In contrast to the extensive studies on ionic liquids, little is known about the basic mechanism of counterion transport in

Received: December 26, 2011
Revised: April 4, 2012
Published: April 18, 2012

Table 1. *Ab Initio* Interaction Energies[a] at 0 K in a Vacuum for 1-Butyl-3-methylimidazolium Cation with Tf_2N^- and PF_6^- Counterions

counteranion	ion pair E_{pair} (kJ/mol)	triple (+) E_{tr+} (kJ/mol)	triple (−) E_{tr-} (kJ/mol)	quadrupole E_{quad} (kJ/mol)	aggregation factor $E_{quad}/2E_{pair}$	pair dipole m_{pair} (D)
PF_6^-	320	417	440	732	1.14	15.1
Tf_2N^-	310	413	415	680	1.10	14.1

[a]All calculations were performed using density functional theory methods with the Gaussian 03 software package. Exchange and correlation were included using the hybrid-GGA B3LYP functional.[50−52]

polymerized ionic liquids. Here, we demonstrate the effect of counterion and tail length on ion migration, aggregation, dielectric constant, and polymer chain dynamics, which provide better understanding of conduction in polymerized imidazolium acrylate polymers. Polymerized ionic liquids are single-ion conductors, and this allows not only a transference number close to unity as required for advanced electrochemical devices but also the absence of concentration polarization of cations that is a common problem encountered in the conventional solid polymeric electrolytes in which both cation and anion are mobile.[41]

To investigate ion and polymer dynamics, the glass transition temperatures (T_g), ionic conductivities, and dielectric constants of these polymers were measured. The dielectric measurement is a particularly powerful tool to investigate the motion of molecules or substituent groups over a broad time range, 10^{-7}–10^2 s.[42,43] Segmental motion of polymers and ionomers are observed in a wide frequency range (mHz to MHz), allowing study over wide temperature ranges.[43] The macroscopic electrode polarization at lower frequencies in dielectric measurements can also be interpreted to determine the number density of conducting ions and their mobility,[44−46] which has recently been utilized with great success for single-ion conductors above T_g.[34,47−49] Our studies of polymer dynamics are complemented by morphology studies using X-ray scattering.

We also compare two ionic liquid counterions: $F_3CSO_2NSO_2CF_3^-$ (referred to as Tf_2N^-) and PF_6^-. Both only bind weakly to imidazolium cations: Table 1 compares 0 K energies[50−52] of formation for ion pairs, positive triple ions, negative triple ions, and quadrupoles of butylmethylimidazolium with Tf_2N^- and PF_6^-. Tf_2N^- binds more weakly than PF_6^-, particularly for the quadrupole energy. Since there is an equilibrium between quadrupoles and two ion pairs, Table 1 also lists the ratio of quadrupole energy to twice the pair energy—a useful gauge of the propensity to aggregate, which is larger for PF_6^- than Tf_2N^-. This is important because it indicates immediately that imidazolium−Tf_2N^- should aggregate less than imidazolium−PF_6^-, and this directly affects the glass transition temperature of these ionomers, with resultant effects on ion conduction.

2. EXPERIMENTAL SECTION

Materials. 2,2′-Azobis(isobutyronitrile) (AIBN, Aldrich Chemical) was recrystallized from chloroform below 40 °C and dried in a vacuum oven. Acetonitrile (MeCN, Aldrich Chemical) for polymerizations was distilled over calcium hydride. Imidazole, 1-bromodecane, *N*-butylimidazole, 11-bromoundecanoic acid, and 4-hydroxybutyl acrylate were purchased from Aldrich Chemical and used as received.

1-Dodecylimidazole. To a solution of imidazole (6.81 g, 100 mmol) in NaOH (50%) solution (8.80 g, 110 mmol), 1-bromododecane (24.92 g, 100 mmol) and tetrahydrofuran (THF) (30 mL) were added. The mixture was refluxed for 3 days. After the mixture had cooled, THF was removed by a rotary evaporator. The residue was extracted with dichloromethane/water 3 times. The combined organic layer was washed with water and then dried over Na_2SO_4. The drying agent was filtered, and the filtrate solution was concentrated. Column chromatography through a short silica gel column with THF gave clear yellow oil (20.51 g, 86.8%).

1-Butyl-3-(10′-carboxydecyl)imidazolium PF_6^- (1a). A mixture of *N*-butylimidazole (6.21 g, 50.0 mmol) and 11-bromoundecanoic acid (13.97 g, 50.0 mmol) in THF (60 mL) was refluxed for 4 days. After the reaction mixture was cooled to room temperature (RT), the precipitated bromide salt was filtered and then washed with cold THF 3 times. The residual brown solid was dissolved in deionized water (100 mL), and KPF_6 (10.12 g, 55 mmol) was added. The mixture was stirred for 24 h at 50 °C. After decanting the upper aqueous layer, the residual oil was washed with deionized water and ethyl ether 3 times each. Drying in a vacuum oven gave a yellow viscous liquid (16.58 g, 73.1%). DSC (−80 to 200 °C, heating and cooling rate 5 K/min in N_2): T_g = −42.2 °C (second cycle), no other transition found.

1-Butyl-3-(10′-carboxydecyl)imidazolium Tf_2N^- (1b). A mixture of *N*-butylimidazole (6.21 g, 50.0 mmol) and 11-bromoundecanoic acid (13.97 g, 50.0 mmol) in THF (120 mL) was refluxed for 4 days. After the reaction mixture was cooled to RT, the precipitated bromide salt was filtered and washed with cold THF 3 times. The filtered solid was dissolved in deionized water (100 mL), and $LiTf_2N$ (15.6 g, 55 mmol) was added. The mixture was stirred for 24 h at 50 °C. After decanting the upper aqueous layer, the precipitated oil was washed with ethyl ether 3 times. The oily product was dissolved in ethyl acetate (EA) (100 mL) and dried over Na_2SO_4. After removing the drying agent by filtration, solvent evaporation and drying in a vacuum oven gave a yellow viscous liquid (19.4 g, 66%). DSC (−80 to 200 °C, heating and cooling rate 5 K/min in N_2): T_g = −55 °C, no other transition found.

1-Dodecyl-3-(10′-carboxydecyl)imidazolium PF_6^- (1c). A mixture of *N*-dodecylimidazole (4.73 g, 20.0 mmol) and 11-bromoundecanoic acid (5.30 g, 20.0 mmol) in MeCN (15 mL) was refluxed for 4 days. After the reaction mixture was cooled to RT, the MeCN was removed by a rotary evaporator. Ethyl ether (80 mL) was added to solidify the residual bromide salt. The precipitate was filtered and washed with ethyl ether 3 times. The colorless crystalline solid (9.02 g, 90%) was obtained after drying in air. The bromide salt (3.55 g, 7.08 mmol) was dispersed in deionized water (200 mL), and KPF_6 (2.76 g, 15 mmol) was added. The mixture was stirred for 24 h at 50 °C. After decanting the upper aqueous layer, the residual oil was washed with deionized water and ethyl ether 3 times each. Drying in a vacuum oven gave a light-yellow viscous liquid (3.95 g, 98% from the bromide salt). The product solidified at RT after several days. DSC (−80 to 200 °C, heating and cooling rate 5 K/min in N_2): T_g = −20.3 °C, T_m = 44 °C (second heating scan).

1-Dodecyl-3-(10′-carboxydecyl)imidazolium Tf_2N^- (1d). From the previous experiment, the bromide salt (5.48 g, 11.0 mmol) was dispersed in deionized water (200 mL), and $LiTf_2N$ (4.58 g, 16 mmol) was added. The mixture was stirred for 24 h at 50 °C. After decanting the upper aqueous layer, the residual oil was washed with deionized water and ethyl ether 3 times each. Drying in a vacuum oven gave a light-yellow viscous liquid (7.65 g, 99% from the bromide salt). DSC (−80 to 200 °C, heating and cooling rate 5 K/min in N_2): T_m = 0 °C (first heating scan) T_g = −57 °C (second heating scan), no other transition found.

1-{ω-[1′-(4″-Acryloyloxy)butoxy]carbonyldecyl}-3-butylimidazolium PF_6^- (2a). A solution of **1a** (2.98 g, 6.56 mmol) in freshly distilled $SOCl_2$ (8 mL) was stirred for 24 h at RT under a N_2 atmosphere. After removing the excess $SOCl_2$ by vacuum, the residue was washed with anhydrous ethyl ether 5 times and then dried by a N_2 stream. The residue (acid chloride of **1a**) was dissolved in dry MeCN (5 mL), and 4-hydroxybutyl acrylate (1.229 g, 8.53 mmol) was added. Into the reaction mixture, triethylamine (0.665 g, 6.56 mmol) was slowly added in an ice bath. The reaction mixture was stirred for 24 h at RT. After water (20 mL) was added, the product was extracted 3 times with EA, and the combined organic layer was dried over anhydrous Na_2SO_4. The drying agent was removed by filtration, and the solvent of the filtrate was removed by a rotary evaporator. The product was rinsed with ethyl ether 5 times with vigorous stirring. Drying in a vacuum oven at RT gave a brown viscous liquid (3.40 g, 89%). DSC (−80 to 60 °C, heating and cooling rate 5 K/min in N_2): T_g = −62 °C, no other transition found.

1-{ω-[1′-(4″-Acryloyloxy)butoxy]carbonyldecyl}-3-butylimidazolium Tf_2N^- (2b). A solution of **1b** (6.150 g, 10.4 mmol) in freshly distilled $SOCl_2$ (12 mL) was stirred for 24 h at RT under a N_2 atmosphere. After removing the excess $SOCl_2$ by vacuum, the residue was washed with anhydrous ethyl ether 5 times and dried by a N_2 stream. The residue (acid chloride of **1b**) was dissolved in dry MeCN (20 mL), and then 4-hydroxybutyl acrylate (1.656 g, 10.9 mmol) was added. Into the reaction mixture, triethylamine (1.052 g, 10.4 mmol) was slowly added in an ice bath. The reaction mixture was stirred for 24 h at RT. After water (20 mL) was added, the product was extracted 3 times with EA, and the combined organic layer was dried over anhydrous Na_2SO_4. The drying agent was removed by filtration, and the solvent of the filtrate was removed by a rotary evaporator. The product was rinsed with ethyl ether 5 times with vigorous stirring. Drying in a vacuum oven at RT gave a yellow viscous oil (3.16 g, 42%). DSC (−80 to 60 °C, heating and cooling rate 5 K/min in N_2): T_g = −69 °C, no other transition found.

1-{ω-[1′-(4″-Acryloyloxy)butoxy]carbonyldecyl}-3-dodecylimidazolium PF_6^- (2c). A solution of **1c** (2.94 g, 5.2 mmol) in freshly distilled $SOCl_2$ (10 mL) was stirred for 24 h at RT under a N_2 atmosphere. After removing the excess $SOCl_2$ by vacuum, the residue was washed with anhydrous ethyl ether 5 times and dried by a N_2 stream. The residue (acid chloride of **1c**) was dissolved in dry MeCN (10 mL), and 4-hydroxybutyl acrylate (0.823 g, 5.7 mmol) was added. Into the reaction mixture, triethylamine (0.578 g, 5.7 mmol) was slowly added in an ice bath. The reaction mixture was stirred for 24 h at RT. After water (20 mL) was added, the product was extracted 3 times with EA, and the combined organic layer was dried over anhydrous Na_2SO_4. The drying agent was removed by filtration, and the solvent was removed by a rotary evaporator. The product was rinsed with ethyl ether 5 times with vigorous stirring. Drying in a vacuum oven at RT gave a brown viscous liquid (3.33 g, 84%). DSC (−80 to 60 °C, heating and cooling rate 5 K/min in N_2): T_m = −24 °C, no other transition found.

1-{ω-[1′-(4″-Acryloyloxy)butoxy]carbonyldecyl}-3-dodecylimidazolium Tf_2N^- (2d). A solution of **1d** (5.31 g, 7.5 mmol) in freshly distilled $SOCl_2$ (12 mL) was stirred for 24 h at RT under a N_2 atmosphere. After removing the excess $SOCl_2$ by vacuum, the residue was washed with anhydrous ethyl ether 5 times and dried by an N_2 stream. The residue (acid chloride of **1d**) was dissolved in dry MeCN (20 mL), and 4-hydroxybutyl acrylate (1.20 g, 8.3 mmol) was added. Into the reaction mixture, triethylamine (0.839 g, 8.3 mmol) was slowly added in an ice bath. The reaction mixture was stirred for 24 h at RT. After water (20 mL) was added, the product was extracted 3 times with EA, and the combined organic layer was dried over anhydrous Na_2SO_4. The drying agent was removed by filtration, and the solvent was removed by a rotary evaporator. The product was rinsed with ethyl ether 5 times with vigorous stirring. Drying in a vacuum oven at RT gave a yellow viscous oil (4.88 g, 79%). DSC (−80 to 60 °C, heating and cooling rate 5 K/min in N_2): T_g = −70 °C, no other transition found.

Radical Polymerizations of Imidazolium Acrylate Monomers. A solution of the imidazolium acrylate monomer and AIBN (2 mol % of the monomer) in degassed MeCN was bubbled with N_2 for 30 min. The solution was stirred for 24 h at 65 °C. After removing MeCN under vacuum, the residue was stirred with EA. Reprecipitation of the resultant solid from acetone into EA was performed 5 times, and the precipitated polymer was washed with deionized water twice. Drying in a vacuum oven at 60 °C gave high-viscosity materials.

4-(Heptanoyloxy)butyl Acrylate (4). To a solution of *n*-heptanoic acid (2.60 g, 20.0 mmol), 4-hydroxybutyl acrylate (1.20 g, 13.0 mmol), and *N,N′*-dicyclohexylcarbodiimide (2.89 g, 14.0 mmol) in dried dichloromethane (10 mL), a solution of 4-(*N,N*-dimethylamino)pyridine (1.71 g, 14.0 mmol) in dichloromethane (5 mL) was slowly added in an ice bath. The reaction mixture was stirred for 12 h at RT. After ethyl ether (40 mL) was added, a precipitate was removed by a short Celite column. The filtrate solution was washed with 1 N HCl solution 3 times, concentrated $NaHCO_3$ 2 times, and water. The organic layer was dried over anhydrous Na_2SO_4. The drying agent was removed by filtration, and the solvent of the filtrate was removed by a rotary evaporator. Drying in a vacuum oven at RT gave colorless oil (3.01 g, 90%).

Radical Polymerization of 4. A mixture of **4** (1.28 g, 5.0 mmol) and AIBN (0.164 g, 0.10 mmol) was bubbled with N_2 for 30 min. The mixture was stirred for 24 h at 65 °C. The polymerization mixture was dissolved in chloroform (5 mL). Precipitation from chloroform into methanol was performed 3 times. Drying in a vacuum oven at 60 °C gave colorless rubbery material (0.833 g, 65% yield). No T_g or T_m in the range of −80 to 200 °C on DSC.

Spectroscopic and Thermal Characterizations. ^1H and ^{13}C NMR spectra were obtained on Varian Inova 400 MHz and Unity 400 MHz spectrometers (results are in Supporting Information). High-resolution electrospray ionization time-of-flight mass spectrometry (HR ESI TOF MS) was carried out on an Agilent 6220 Accurate Mass TOF LC/MS spectrometer in positive ion mode. Differential scanning calorimetry (DSC) with heating and cooling rates of 5 or 10 K/min on ∼10 mg samples was done using a TA Instruments Q2000 differential scanning calorimeter (see Supporting Information Figure S11). The thermal stabilities of these polymers were studied by thermogravimetric analysis (TGA) under N_2 using a TA Instruments Q500 thermogravimetric analyzer at a heating rate of 10 K/min heating under N_2 purge.

Dielectric Spectroscopy. The dielectric measurements of the polymers were performed by dielectric relaxation spectroscopy. Samples were prepared for the dielectric measurement by allowing them to flow to cover a 30 mm diameter freshly polished brass electrode at 100 °C *in vacuo*. To control the sample thickness at 50 μm, silica spacers were placed on top of the sample after it flowed to cover the electrode. Then a 15 mm diameter freshly polished brass electrode was placed on top to make a parallel plate capacitor cell which was squeezed to a gap of 50 μm in the instrument (with precise thickness checked after dielectric measurements were complete). The ionomers sandwiched between two electrodes were positioned in a Novocontrol GmbH Concept 40 broadband dielectric spectrometer, after being in a vacuum oven at 100 °C for 24 h. Each sample was then annealed in the Novocontrol at 120 °C in a heated stream of nitrogen for 1 h prior to measurements. The dielectric permittivity was measured using a sinusoidal voltage with amplitude 0.1 V and 10^{-2}–10^7 Hz frequency range for all experiments. Data were collected in isothermal frequency sweeps every 5 K, from 120 °C to near T_g.

X-ray Scattering. X-ray scattering was performed with a multi-angle X-ray scattering system that generates Cu Kα X-rays, λ = 0.154 nm, from a Nonius FR 591 rotating anode operated at 40 kV and 85 mA. The bright, highly collimated beam was obtained via Osmic Max-Flux optics and pinhole collimation in an integral vacuum system. The scattering data were collected using a Bruker Hi-Star two-dimensional detector with a sample-to-detector distance of 11 cm. To minimize the exposure of the materials to moisture, previously dried samples were inserted into 1 mm glass capillaries under vacuum at elevated temperatures from RT to 110 °C. As the samples flowed into the capillary under vacuum, bubbles were eliminated. The filled capillaries were cooled to RT under vacuum. Scans were performed from RT to 120 °C, controlling the temperature in situ using a Linkam

Scheme 1. Synthesis of Poly(*N*-alkylimidazolium acrylate)s 3a−d

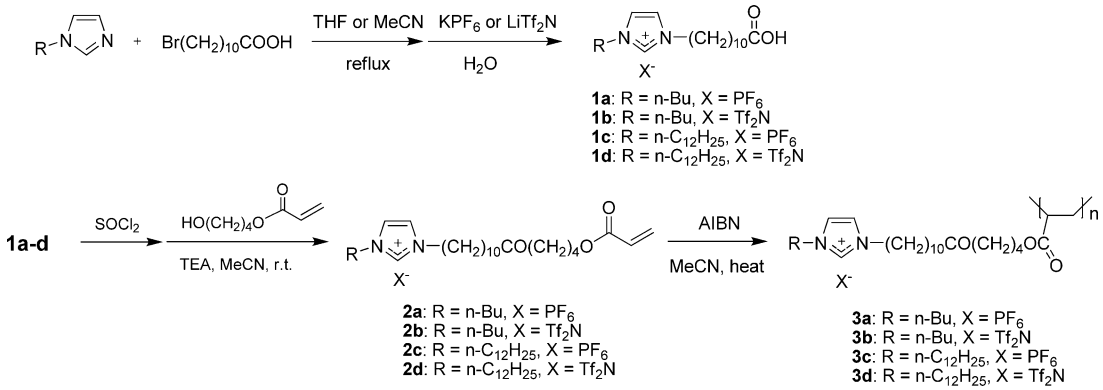

Scheme 2. Synthesis of Nonionic Polymer 5

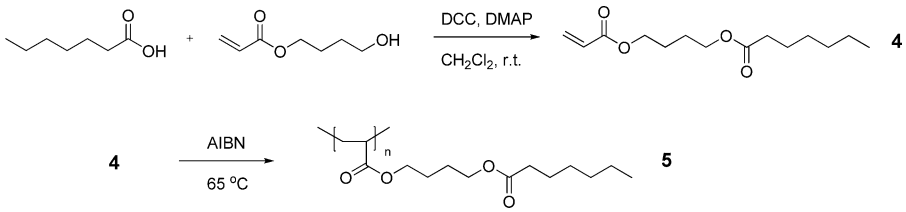

Table 2. DSC, DRS, and TGA Thermal Analysis, Total Ion Concentration p_0, Refractive Index n, and Fragility m of Ionomers

sample	DSC T_g (K)	DRS[a] T_g (K)	TGA (°C) 5% w/w loss	p_0[b] ($\times 10^{20}$ cm^{-3})	n[b]	m[c] ± 6
C_4-PF_6 (3a)	256	248	341	12.1	1.461	105
C_4-Tf_2N (3b)	230	222	382	10.3	1.462	115
C_{12}-PF_6 (3c)	244	245	340	9.62	1.468	83
C_{12}-Tf_2N (3d)	226	221	336	8.46	1.469	88

[a] T_g determined from dielectric spectroscopy (defined at $\omega_a(T_g) = 10^{-2}$ rad/s). [b] Total ion concentration and refractive index from group contribution method based on structure.[55] [c] m determined from eq 15 using the VFT fit parameters for the segmental (α) peak frequency (open symbols in Figure 8a).

temperature control stage with a step size of ∼30 K and heating and cooling rates of 10 K/min. Adjustments were made to the set temperature of the heating device so that the temperature of the sample inside the glass capillary would equal the desired temperature. The samples were equilibrated at each temperature for 10 min before starting the X-ray data collection. The X-ray scattering profiles were evaluated using Datasqueeze software.[53] The intensities were first corrected for primary beam intensity, and background scattering from an empty 1 mm glass capillary was subtracted. Intensities were not corrected for sample density. The isotropic 2-D scattering patterns were azimuthally integrated to yield intensity versus scattering angle.

3. RESULTS AND DISCUSSION

A. Ionomer Synthesis. We synthesized new acrylate monomers and polymers with ionic imidazolium units, as depicted in Scheme 1. The quarternization reactions of 1-alkylimidazole and ω-bromoalkanoic acids gave water-soluble carboxy-terminated imidazolium salts. Ion exchange from the bromide salts to hexafluorophosphate (PF_6^-) or bis-(trifluoromethanesulfonyl)imide (Tf_2N^-) counterions was done in water with excess KPF_6 or $LiTf_2N$. To confirm the essentially complete removal of the bromide ions from the imidazolium salts, a Beilstein copper/flame test[54] was performed before the next reaction. The polymerizable acrylate unit was introduced by the esterification of the imidazolium carboxyl salts with 4-hydroxybutyl acrylate. The imidazolium acrylate monomers (**2a−d**) are soluble in acetone, MeCN, DMF, and ethyl acetate (EA), but not soluble in either diethyl ether or water. To prevent a self-polymerization, all monomers were stored in a freezer (<0 °C) after packing with dry N_2.

The radical polymerization of the monomers was done with 2,2′-azobis(isobutyronitrile) (AIBN) in MeCN. The product polymers were purified by precipitation from EA, which is a good solvent for the monomers but does not dissolve the polymers. After purification, the water contents of the polymers were checked by ^{1}H NMR spectroscopy. In the ^{1}H NMR spectra (see Supporting Information) the vinyl protons of the monomers disappeared in the purified polymers, and the polymers exhibited some peak broadening. The CH_2 protons that are close to the polymer backbone were broadened, whereas the alkyl protons which are well removed from the polymer backbone still appear as sharp signals because carbon−carbon bond rotation is much faster in the alkyl chains which are far from the polymer backbone and they remained sharp.

To compare the dielectric properties, nonionic polymer **5** was prepared similarly to the imidazolium ionomers as shown in Scheme 2. After coupling heptanoic acid and 4-hydroxybutyl acrylate to form monomer **4**, the polymerization of **4** was performed with AIBN without any solvent. The nonionic polymer **5** was purified by several precipitations from its chloroform solution to methanol with vigorous stirring. The nonionic polymer **5** is a rubbery elastomer; however, it does not show a glass transition in DSC down to −80 °C.

B. Thermal Analysis. The new imidazolium pendant homopolymers each have a single glass transition, as reported

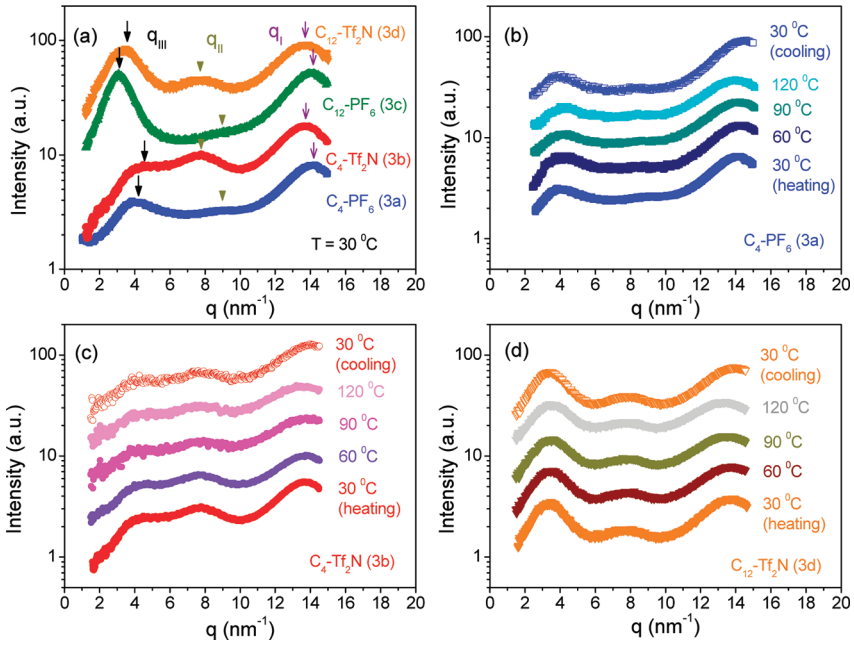

Figure 1. X-ray scattering intensity as a function of scattering wavevector q for (a) the imidazolium-based ionomers at room temperature and (b) **C_4-PF_6 (3a)**, (c) **C_4-Tf_2N (3b)**, and (d) **C_{12}-Tf_2N (3d)**, each at four temperatures (30, 60, 90, and 120 °C). The arrows indicate peaks that correspond to the amorphous halo (q_I), anion−anion correlations (q_{II}), and separation between ionic aggregates (q_{III}). The intensity of the ionic aggregation spacing peak (q_{III}) increases enormously as the tail length increases from *n*-butyl to *n*-dodecyl, which we interpret to signify that dodecyl tails favor ion aggregation. The data were shifted on the log intensity scale for clarity.

in Table 2. The polymers do not display crystallization or melting in the temperature range of −80 to 200 °C by DSC. Replacing PF_6^- with Tf_2N^- consistently lowered T_g by ∼22 K. The Tf_2N^- counterion has previously been shown to act at a plasticizer for imidazolium ionic liquids[9,18] and their polymers.[27,33,34] Since association of ion pairs allows them to act as temporary cross-links that raise T_g, the more strongly associating PF_6^- imparts higher T_g than Tf_2N^- for the poly(imidazolium acrylate)s, as anticipated from the *ab initio* results of Table 1. The length of tail also affects the T_g determined by DSC (denoted DSC T_g): ionomers with *n*-dodecyl tails exhibit slightly (∼8 K) lower DSC T_gs than those with *n*-butyl tails. However, the T_g, obtained by dielectric spectroscopy as the temperature at which the peak segmental relaxation time was 100 s (denoted DRS T_g; listed in Table 2[55]), shows no effect of tail length between ionomers with *n*-dodecyl tails and with *n*-butyl tails. TGA under nitrogen at 10 K/min suggests that all four ionomers are thermally stable at least until 300 °C.

C. X-ray Scattering. Figure 1a compares the room temperature X-ray scattering profiles for the four imidazolium acrylate ionomers with different side chain tail lengths and counterions. Three distinct peaks are observed: the higher-angle peak at $q_I \approx 14$ nm^{-1} corresponds to the amorphous halo, the more subtle intermediate-angle peak at $q_{II} \approx 8$ nm^{-1} is attributed to correlation between the anions,[56,57] and the lower-angle peak at $q_{III} \approx 2$ nm^{-1} for the ionomers with *n*-dodecyl tails and $q_{III} \approx 4$ nm^{-1} for the ionomers with *n*-butyl tails indicates the spacing between ion aggregates.[58] For the amorphous halos at q_I, the peak slightly shifts to lower wavevector as the size of anion increases from PF_6^- to Tf_2N^-. A similar shift is also observed for the anion−anion scattering peak at q_{II}. However, both q_I and q_{II} peaks appear at the same position as the tail length increases from *n*-butyl to *n*-dodecyl. In contrast, the ionic aggregation scattering peak at q_{III} shifts to lower q and its intensity increases significantly, as the tail length increases from *n*-butyl to *n*-dodecyl. The ionomer peak (q_{III}) intensity arises from both the uniformity of the interaggregate spacing and the electron density difference between the matrix and the ionic aggregates.[59] Both the peak positions and peak intensities remain nearly the same with increasing temperature as shown in Figures 1b,c,d. Morphological studies of 1-alkyl-3-methylimidazolium PF_6^- or Tf_2N^- ionic liquids as a function of the alkyl chain length by means of neutron scattering[60] and molecular dynamics simulation[38,61] observed quite similar ion aggregation: ionic liquids with long side chains exhibit a bicontinuous morphology, one region consisting of polar moieties (anion/cation pairs and aggregates) and the other consisting of nonpolar alkyl tails.

D. Ionic Conductivity. To understand the influence of anions and tail length on ionic conductivity, the temperature dependence of DC conductivity shown in Figure 2 is evaluated from a roughly 3 decade frequency range where the in-phase part of the conductivity $\sigma'(\omega) = \varepsilon''(\omega)\varepsilon_0\omega$ is independent of frequency, as shown in Figure 3. The inset in Figure 2 shows the strong correlation between ionic conductivity at 25 °C and T_g for these monomers and their polymers. As expected, monomers with lower T_g show higher ionic conductivity than the polymers with higher T_g. There also exists a significant effect from different anions on ionic conductivity for these ionomers. Because of the suppression in the T_g, the larger Tf_2N^- anion raises the ionic conductivity of **C_4-Tf_2N (3b)** and **C_{12}-Tf_2N (3d)** by ∼100× at room temperature, compared to the PF_6^- ionomers (**C_4-PF_6 (3a)** and **C_{12}-PF_6 (3c)**). However, an effect from the *n*-dodecyl vs *n*-butyl tail on ionic conductivity is more subtle; that is, ionomers with shorter tail (**C_4-PF_6 (3a)** and **C_4-Tf_2N (3b)**) showed slightly higher ionic conductivity in spite of having higher T_g. In order to better understand counterion conduction, it is necessary to distinguish whether the increase in ionic conductivity is due to a larger number

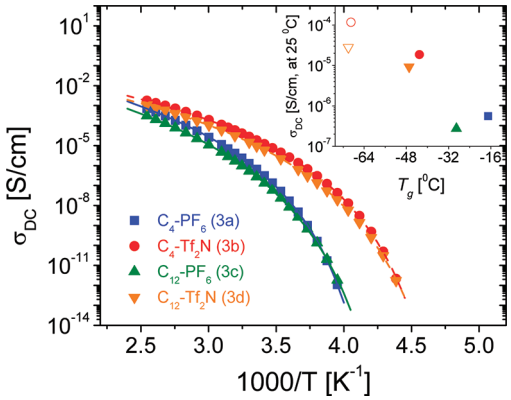

Figure 2. Temperature dependence of ionic conductivity for PF_6^- and Tf_2N^- ionomers. Tf_2N^- (**C_4-Tf_2N (3b)** and **C_{12}-Tf_2N (3d)**) ionomers have consistently higher conductivities than PF_6^- (**C_4-PF_6 (3a)** and **C_{12}-PF_6 (3c)**) ionomers. Solid and dashed curves are eq 16 with all parameters fixed (values in Tables 3 and 4): E_a and p_∞ are determined by an Arrhenius fit to simultaneously conducting ion content p (Figure 4), while μ_∞, D, and T_0 are determined by a VFT fit to simultaneously conducting ion mobility μ (Figure 5). The inset shows ionic conductivity at room temperature as a function of glass transition temperature for these four ionomers (**3a** (■), **3b** (●), **3c** (▲), and **3d** (▼)) and two monomers (**2b** (○) and **2d** (▽)).

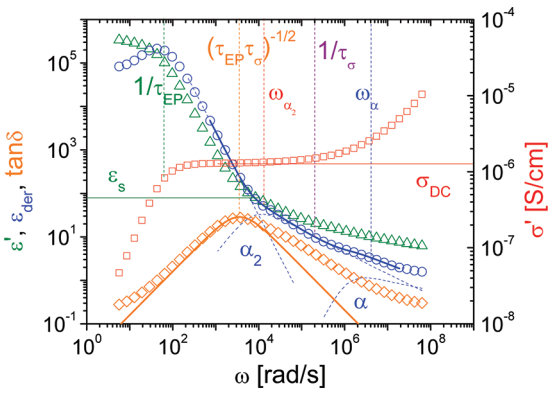

Figure 3. Dielectric response of imidazolium-based ionomer **C_4-Tf_2N (3b)** to applied AC field at 273 K. The dielectric loss derivative function ε_{der} (blue circles) shows two relaxation processes: segmental motion (α) at ω_α and ions exchanging states (α_2) at $\omega_{\alpha 2}$. After ion motion becomes diffusive at τ_σ, the α_2 process not only contributes to DC conductivity σ_{DC}, noted as the plateau region in the in-phase part of conductivity σ' (red squares), but also enhances the static dielectric constant ε_s in the dielectric permittivity function ε' (green triangles). The peak of the loss tangent tanδ (orange diamonds) gives the geometric mean of the time scales of conductivity and electrode polarization $(\tau_{EP}\tau_\sigma)^{1/2}$, then determining the number density of simultaneously conducting ions p and their mobility μ.

density of simultaneously conducting ions p or to an increase in their mobility μ.

E. Electrode Polarization Analysis. A physical model of electrode polarization (EP) makes it possible to separate ionic conductivity into the number density of simultaneously conducting ions and their mobility,[44−46,62,63] as has recently been done for other single-ion conductors above T_g.[34,47−49,64,65] Electrode polarization occurs at low frequencies, where the transporting ions have sufficient time to polarize at the blocking electrodes during the cycle. That polarization manifests itself in (1) an increase in the effective capacitance of the cell (increasing the apparent dielectric constant) and (2) a decrease in the in-phase part of the conductivity, as the polarizing ions reduce the field experienced by the transporting ions. The natural time scale for conduction is the time when counterion motion becomes diffusive.

$$\tau_\sigma \equiv \frac{\varepsilon_s \varepsilon_0}{\sigma_{DC}} \tag{1}$$

At low frequencies the conducting ions start to polarize at the electrodes and fully polarize at the electrode polarization time scale

$$\tau_{EP} \equiv \frac{\varepsilon_{EP} \varepsilon_0}{\sigma_{DC}} \tag{2}$$

wherein ε_{EP} is the (considerably larger) effective permittivity after the electrode polarization is complete (see Figure 3). The Macdonald and Coelho model[44−47,62,63] treats electrode polarization as a simple Debye relaxation with loss tangent,

$$\tan\delta = \frac{\omega\tau_{EP}}{1 + \omega^2\tau_\sigma\tau_{EP}} \tag{3}$$

allowing a two-parameter fit to determine the electrode polarization time τ_{EP} and the conductivity time τ_σ. The Macdonald and Coelho model then determines the number density of simultaneously conducting ions p and their mobility μ from τ_{EP} and τ_σ

$$p = \frac{1}{\pi l_B L^2}\left(\frac{\tau_{EP}}{\tau_\sigma}\right)^2 \tag{4}$$

$$\mu = \frac{eL^2\tau_\sigma}{4\tau_{EP}^2 kT} \tag{5}$$

wherein $l_B \equiv e^2/(4\pi\varepsilon_s\varepsilon_0 kT)$ is the Bjerrum length, L is the spacing between electrodes, k is the Boltzmann constant, and T is absolute temperature.

Conducting Ion Content. The temperature dependence of the number density of simultaneously conducting ions p calculated from eq 4 is plotted in Figure 4, and the fraction of ions participating in conduction (p/p_0 wherein p_0, listed in

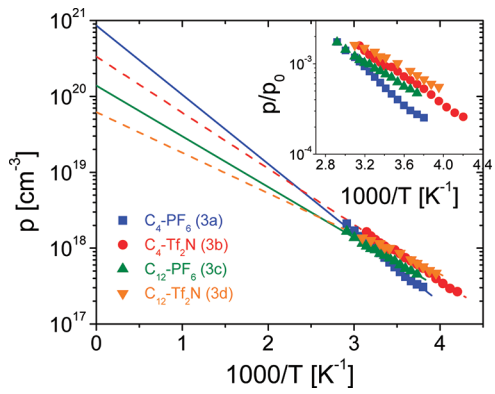

Figure 4. Temperature dependence of simultaneously conducting ion concentration p. Solid (PF_6^- ionomers) and dashed (Tf_2N^- ionomers) lines are Arrhenius fits to eq 6 with two fitting parameters (E_a and p_∞, listed in Table 3). The observation that ionomers with the n-dodecyl tails have much lower p_∞ than ionomers with the n-butyl tails suggests that the n-dodecyl tails aggregate ions. The inset displays the fraction of anions simultaneously participating in conduction (p divided by the total anion concentration p_0).

Table 2, is the total anion number density[55]) is shown in the Figure 4 inset. The temperature dependence of simultaneously conducting ion concentration for these imidazolium-based ionomers is well described by an Arrhenius equation

$$p = p_\infty \exp\left(-\frac{E_a}{RT}\right) \tag{6}$$

wherein p_∞ and E_a, listed in Table 3, are the conducting ion concentration as $T \to \infty$ and the activation energy for conducting ions, respectively. The fact that for some ionomers p_∞ is smaller than p_0 indicates some of the counterions are too strongly aggregated to participate in ionic conduction, and $1 - p_\infty/p_0$ (listed in Table 3), tells us the fraction of counterions that are trapped and are unable to participate in conduction.[65] The observation that ionomers with *n*-dodecyl tails have much higher fraction of trapped ions than ionomers with *n*-butyl tails suggests that **C_{12}-PF_6 (3c)** and **C_{12}-Tf_2N (3d)** exhibit stronger ionic aggregation than **C_4-PF_6 (3a)** and **C_4-Tf_2N (3b)**, consistent with the stronger q_{III} peak in X-ray scattering in section 3C and the analysis of the static dielectric constant in section 3F. The activation energies for the PF_6^- ionomers (**C_4-PF_6 (3a)** and **C_{12}-PF_6 (3c)**) are higher than those for the Tf_2N^- ionomers (**C_4-Tf_2N (3b)** and **C_{12}-Tf_2N (3d)**), indicating a lower binding energy for the imidazolium ions with the larger Tf_2N^- ions than for the PF_6^- ions,[31] as anticipated by the *ab initio* calculations presented in Table 1. The length of tail also affects the activation energy; ionomers with *n*-dodecyl tails exhibit lower activation energies of the simultaneously conducting ions than those with *n*-butyl tails. Without microphase separation, the nonpolar *n*-butyl tails are included in the dielectric constant of the surroundings, but when the *n*-dodecyl tails microphase separate, they no longer lower the dielectric constant in the phase where the ions reside. This effectively means that the dielectric constants (before ions move) are larger for ionomers with *n*-dodecyl tails than for those with *n*-butyl tails, lowering the effective activation energy for ion motion.

Table 3. Fitting Parameters (Eq 6) for the Temperature Dependence of the Number Density of Simultaneously Conducting Ions

		conducting ion concentration		
sample	$\log(p_0)$ (cm^{-3})	$\log(p_\infty)$ (cm^{-3})	E_a (kJ/mol)	$1 - p_\infty/p_0$
C_4-PF_6 (3a)	21.1	20.9	17.5	0.29
C_4-Tf_2N (3b)	21.0	20.5	14.1	0.68
C_{12}-PF_6 (3c)	21.0	20.1	12.8	0.86
C_{12}-Tf_2N (3d)	20.9	19.8	10.2	0.93

The inset in Figure 4 indicates that the fraction of counterions simultaneously participating in conduction (p/p_0) in these single-ion conductors is quite low, <0.1% of the total number of counterions, except at the highest temperatures studied. The conducting ion content evaluated from the EP model is the number density of ions in a conducting state in any snapshot, which sets the boundary condition for the solution of the Poisson−Boltzmann equation. Only a small fraction of total ions is in a conducting state at any given instant in time, similar to observations on other single-ion conducting ionomers with alkali metal counterions[47−49] or ionic liquid counterions.[34,64,65]

Mobility of Conducting Ions. The temperature dependence of the mobility of the simultaneously conducting ions determined from the EP model is displayed in Figure 5 as the filled symbols. Since conductivity can be measured over a far wider temperature range, we divide the DC conductivity data in Figure 2 by the elementary charge *e* and by the Arrhenius fit to eq 6 of simultaneously conducting ion number density *p* to determine an extended mobility, plotted in Figure 5 as the open symbols. Both mobility and extended mobility are then fit to the Vogel−Fulcher−Tammann (VFT) equation,

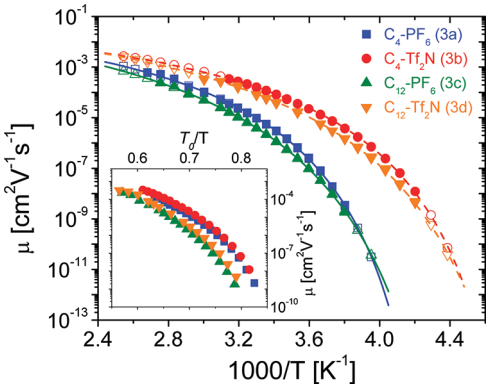

Figure 5. Temperature dependence of simultaneously conducting ion mobilities for PF_6^- and Tf_2N^- ionomers, determined from (1) the EP model (filled symbols) and (2) dividing the DC conductivity data by the product of the elementary charge *e* and the Arrhenius fit to eq 6 of simultaneously conducting ion number density *p* (open symbols, referred to as extended mobility). Both mobility and extended mobility are fit to eq 7 as solid and dashed curves. Tf_2N^- ionomers (**C_4-Tf_2N (3b)** and **C_{12}-Tf_2N (3d)**) have consistently higher mobilities than PF_6^- ionomers (**C_4-PF_6 (3a)** and **C_{12}-PF_6 (3c)**). The inset shows the ionic mobilities with respect to inverse temperature normalized by T_0, indicating that ionomers with *n*-butyl tails have higher mobilities than those with *n*-dodecyl tails.

$$\mu = \mu_\infty \exp\left(-\frac{DT_0}{T - T_0}\right) \tag{7}$$

wherein μ_∞ is the highest temperature limit of the mobility, T_0 is the Vogel temperature, and *D* is the so-called strength parameter (reciprocally related to fragility *m*). The ionic mobilities of Tf_2N^- in **C_4-Tf_2N (3b)** and **C_{12}-Tf_2N (3d)** are higher than those of PF_6^- in **C_4-PF_6 (3a)** and **C_{12}-PF_6 (3c)** because the larger Tf_2N^- anion imparts lower T_g. To understand the effect of tail length, the mobilities are also plotted against T_0/T (see inset of Figure 5). The data do not merge into a single curve but instead yield two separate curves. The ionomers with shorter tails (**C_4-PF_6 (3a)** and **C_4-Tf_2N (3b)**) have somewhat higher mobilities than those with longer tails (**C_{12}-PF_6 (3c)** and **C_{12}-Tf_2N (3d)**) for the same T_0/T. Similar results were reported for pure ionic liquids,[11,66] whereby increasing the alkyl chain length from butyl to hexyl to octyl increases the viscosity of ionic liquids based on 1-alkyl-3-methylimidazolium with a Tf_2N^- anion. Since the VFT temperature dependence of ion mobility reflects the coupling of segmental motion and ion transport, the lower ion mobility in our ionomers with C_{12} is likely caused by their slower segmental motion due to their stronger ion aggregation, seen in the X-ray data in Figure 1.

F. Static Dielectric Constant. The static dielectric constant ε_s is defined as the low-frequency plateau of $\varepsilon'(\omega)$ before EP begins, shown in Figure 3 and calculated using eq 1 from the measured σ_{DC} and τ_σ obtained from fitting EP to eq 3.[47,64,65] Figure 6 displays the static dielectric constant for these imidazolium-based ionomers and the nonionic polymer **5** vs inverse temperature. The nonionic polymer **5** having no imidazolium cation nor anion exhibits $\varepsilon_s = 8$ at room temperature. ε_s for the ionomers with imidazolium cation and either PF_6^- or Tf_2N^- anion is much larger, especially for those with *n*-butyl tails (**C_4-PF_6 (3a)** and **C_4-Tf_2N (3b)**) with $\varepsilon_s \approx 80$ at the lowest temperatures studied. As the tail length increases from butyl to dodecyl, ε_s in **C_{12}-PF_6 (3c)** and **C_{12}-Tf_2N (3d)** significantly decreases.

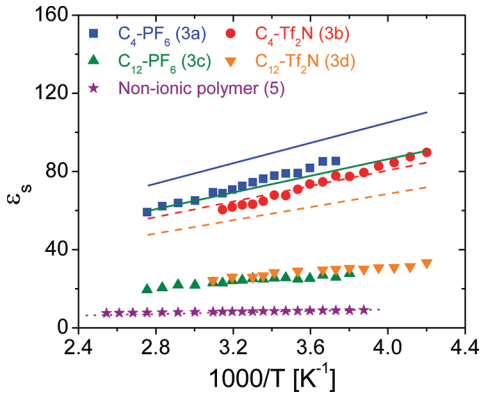

Figure 6. Temperature dependence of static dielectric constant ε_s for imidazolium-based ionomers and a nonionic polymer. The lines are predictions of the Onsager equation with fixed concentration and strength of dipoles: the purple dotted line is eq 8 for nonionic polymer **5** with $\sum_i \nu_i m_i^2/(9\varepsilon_0 k) = 249$ K as the sole fitting parameter, and the colored solid and dashed lines are eq 9 for the four imidazolium-based ionomers, assuming all ions exist as isolated contact pairs ($\nu_{pair} = p_0$) with dipoles given by the *ab initio* estimates in Table 1 and assuming the Kirkwood correlation factor $g = 1$.

The temperature dependence of ε_s for the nonionic polymer can be understood through the Onsager equation[67−69]

$$\left[\frac{(\varepsilon_s - \varepsilon_\infty)(2\varepsilon_s + \varepsilon_\infty)}{\varepsilon_s(\varepsilon_\infty + 2)^2}\right]_{\text{nonionic}} = \frac{1}{9\varepsilon_0 kT}\sum_i \nu_i m_i^2 \tag{8}$$

wherein ν_i is the number density of dipoles, m_i is their dipole moment, and ε_∞ is the high-frequency limit of the dielectric constant (here taken to be an approximate value of $\varepsilon_\infty = n^2$, where n is the refractive index, listed in Table 2). The purple dotted line in Figure 6 is fit to eq 8 with the $\sum_i \nu_i m_i^2$ term as the sole fitting parameter, showing that ε_s of the nonionic polymer **5** is well described by the Onsager equation. The polymerized ionic liquids have an imidazolium cation attached to each side chain with the associated anion (PF_6^- or Tf_2N^-) and for such ionomers the contribution of the ions to the static dielectric constant can be analyzed[49,59] by simply adding the effect of ion pairs to eq 8:

$$\left[\frac{(\varepsilon_s - \varepsilon_\infty)(2\varepsilon_s + \varepsilon_\infty)}{\varepsilon_s(\varepsilon_\infty + 2)^2}\right]_{\text{ionomer}} = \frac{\nu_{pair} m_{pair}^2}{9\varepsilon_0 kT} + \left[\frac{(\varepsilon_s - \varepsilon_\infty)(2\varepsilon_s + \varepsilon_\infty)}{\varepsilon_s(\varepsilon_\infty + 2)^2}\right]_{\text{nonionic}} \tag{9}$$

wherein ν_{pair} is the number density of ion pairs and m_{pair} is their dipole moment. The solid and dashed lines in Figure 6 are the Onsager predictions of eq 9 for each ionomer, assuming all ions are in the isolated ion pair state ($\nu_{pair} = p_0$, listed in Table 2) with the contact pair dipole from *ab initio* listed in Table 1. Starting at the top of Figure 6, the Onsager prediction for the ionomers with *n*-butyl tails, **C_4-PF_6 (3a)** and **C_4-Tf_2N (3b)**, agree reasonably with their measured ε_s. The Onsager equation predicts that the dielectric constant decreases as temperature increases (as $1/T$) from thermal randomization. The Onsager prediction for **C_4-PF_6 (3a)** is ∼13% above the measured dielectric constant, presumably indicating that the dipole of the ion pairs for imidazolium-PF_6 is overestimated by ∼7% in our *ab initio* calculations (Table 1). Although the ionomers with *n*-dodecyl tails exhibit dielectric constants that parallel the Onsager prediction of eq 9, **C_{12}-PF_6 (3c)** and **C_{12}-Tf_2N (3d)** show nearly identical dielectric constants across the entire temperature range, which are more than a factor of 2 below the Onsager prediction of eq 9. Those ionomers with *n*-dodecyl tails are still significantly more polar than the nonionic polymer **5**, but many of their ions are aggregated, analogous to lithium sulfonate−PEO ionomers.[59]

Another way to view ion aggregation is that this effectively correlates neighboring dipoles of ion pairs. Correlation of neighboring dipoles was considered by Kirkwood[70,71] and Fröhlich[69] by introducing a prefactor g into eq 9, and this idea is extensively utilized.[42,68,69] For example, the dielectric constants for highly associating liquids such as acids, alcohols, and water are underestimated by the Onsager theory.[71] On the other hand, molecules with internal hindered rotation or restricted rotational degrees of freedom that prohibit alignment with the field cannot fully respond to the field as expected from their individual dipole moments, and therefore, the Onsager model overestimates the resulting dielectric constant.[72]

$$g = \frac{9\varepsilon_0 kT}{\nu_{pair} m_{pair}^2}\left\{\frac{(\varepsilon_s - \varepsilon_\infty)(2\varepsilon_s + \varepsilon_\infty)}{\varepsilon_s(\varepsilon_\infty + 2)^2} - \left[\frac{(\varepsilon_s - \varepsilon_\infty)(2\varepsilon_s + \varepsilon_\infty)}{\varepsilon_s(\varepsilon_\infty + 2)^2}\right]_{\text{nonionic}}\right\} \tag{10}$$

If there are no specific correlations, $g = 1$ and the Kirkwood−Fröhlich equation reduces to the Onsager equation. For polar liquids in which dipoles tend to orient with parallel dipole alignments, $g > 1$. For example, hydrogen bonding in water makes $g = 2.9$ at 0 °C, decreasing steadily as temperature is increased, to $g = 2.3$ at 100 °C. When dipoles either prefer antiparallel alignment or a significant fraction of dipoles are unable to move in response to the field, $g < 1$. The g factor can be calculated from eq 10 by assuming that all ions are in the isolated contact pair state ($\nu_{pair} = p_0$ where p_0, listed in Table 2, is the total anion number density) with the contact pair dipole from *ab initio* listed in Table 1. Our imidazolium ionomers exhibit apparent Kirkwood correlation factors $0.8 < g < 1.1$ for ionomers with *n*-butyl tails and $0.2 < g < 0.4$ for ionomers with *n*-dodecyl tails, over the whole temperature range studied. This can explain the strong increase in intensity of the ionic aggregate scattering peak in the X-ray data of Figure 1, as the tail length increases from *n*-butyl to *n*-dodecyl. Ionic aggregation makes $g \ll 1$ for the ionomers with *n*-dodecyl tails while $g \cong 1$ for the ionomers with *n*-butyl tails.

G. Dielectric Relaxations. In addition to ion conduction of these ionomers, to assess the effect of anions and tail length on polymer chain or ion dynamics, the loss peaks of dipolar relaxation processes are evaluated. However, electrode polarization and conduction can obscure the loss peaks of interest that are due to ion motion or segmental relaxation.[43] Thus, we use the derivative formalism[73] which eliminates the conductivity contribution from loss spectra to elucidate relaxation processes in the temperature range where EP and conductivity dominate.[48,49]

$$\varepsilon_{\mathrm{der}} = -\frac{\pi}{2}\frac{\partial\varepsilon'(\omega)}{\partial \ln \omega} \tag{11}$$

In the derivative spectra of Figure 7, these imidazolium-based ionomers exhibit two dielectric relaxations designated as α and α_2 in the order of decreasing frequency. The dipolar relaxations were further explored by fitting the derivative spectra with one power law for EP plus two Havriliak−Negami (HN) functions for those two dielectric relaxations

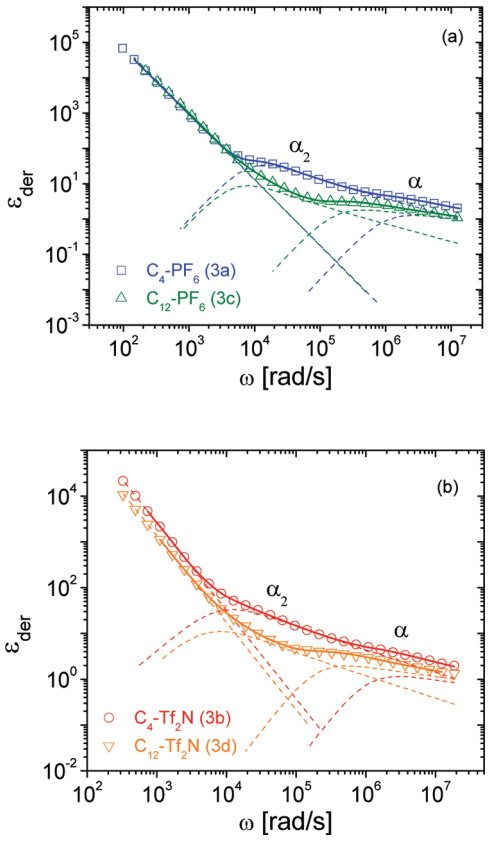

Figure 7. Dielectric loss derivative spectra fit (solid lines) to the sum of a power law for EP and two derivative forms of the HN function for ion rearrangement and polymer segmental motion of (a) PF_6^- ionomers (**C_4-PF_6 (3a)** and **C_{12}-PF_6 (3c)**) at 303 K and (b) Tf_2N^- ionomers (**C_4-Tf_2N (3b)** and **C_{12}-Tf_2N (3d)**) at 273 K. Two relaxation processes (α_2 at lower frequency and α at higher frequency) are observed, and individual contributions of the relaxations are shown as dashed lines. The solid curves are five-parameter fits to eq 12 with fixed values of the EP power law slope[76] (s) and shape parameters of the two HN functions (a and b) for (a) PF_6^- ionomers: $s = 1.88$, $a_{\alpha 2} = 1.0$, $b_{\alpha 2} = 0.5$, $a_\alpha = 1.0$, and $b_\alpha = 0.2$ and for (b) Tf_2N^- ionomers: $s = 1.91$, $a_{\alpha 2} = 0.88$, $b_{\alpha 2} = 0.55$, $a_\alpha = 1.0$, and $b_\alpha = 0.2$.

$$\varepsilon_{\mathrm{der}} = A\omega^{-s} - \frac{\pi}{2}\left(\left[\frac{\partial\varepsilon'_{\mathrm{HN}}(\omega)}{\partial \ln \omega}\right]_{\alpha_2} + \left[\frac{\partial\varepsilon'_{\mathrm{HN}}(\omega)}{\partial \ln \omega}\right]_{\alpha}\right) \tag{12}$$

with

$$\varepsilon'_{\mathrm{HN}}(\omega) = \mathrm{Real}\left\{\frac{\Delta\varepsilon}{[1 + (i\omega/\omega_{\mathrm{HN}})^a]^b}\right\}$$

wherein A and s are constants, $\Delta\varepsilon$ is the relaxation strength, a and b are shape parameters, and ω_{HN} is a characteristic frequency related to the frequency of maximal loss $\omega_{\max}$ by[43,74,75]

$$\omega_{\max} = \omega_{\mathrm{HN}}\left(\sin\frac{a\pi}{2+2b}\right)^{1/a}\left(\sin\frac{ab\pi}{2+2b}\right)^{-1/a} \tag{13}$$

In each fit of the ionomer derivative spectrum at each temperature, five of the ten parameters in eq 12 are fixed (EP power law exponent[76] s and the two sets of HN shape parameters a and b) to values given in the Figure 7 caption, and the relaxation strengths are constrained with $\Delta\varepsilon_{\alpha_2} + \Delta\varepsilon_\alpha + \varepsilon_\infty = \varepsilon_s$. The peak relaxation frequency $\omega_{\max}$ and relaxation strength $\Delta\varepsilon$ of the α and α_2 processes are determined from this fitting, and their temperature dependences are displayed in Figure 8. In ionic liquids, dielectric relaxation processes from motions of anions and cations are observed.[77,78] Ionomers exhibit two

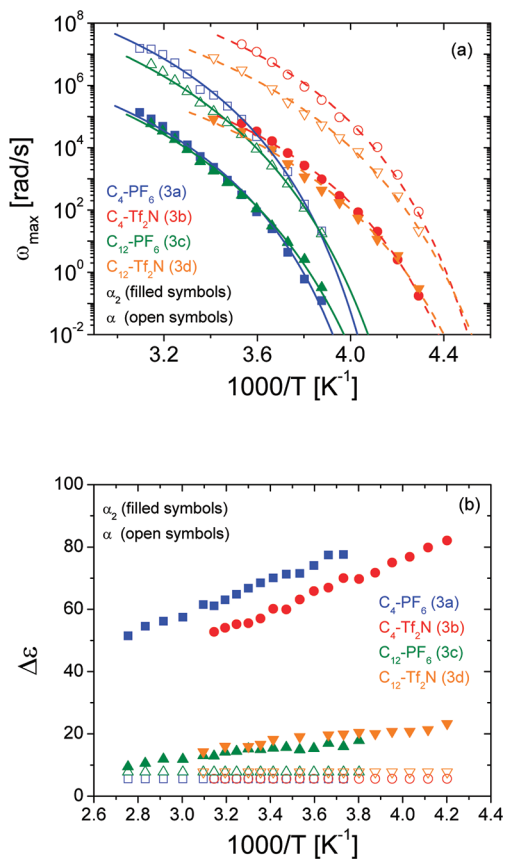

Figure 8. Temperature dependence of (a) relaxation frequency maxima $\omega_{\max}$ and (b) relaxation strengths $\Delta\varepsilon$ of the α (open symbols) and α_2 (filled symbols) processes. The solid (PF_6^- ionomers) and dashed (Tf_2N^- ionomers) curves are fits of the VFT equation (eq 14) using T_0 from the mobility VFT fits in Figure 5.

Table 4. Fitting Parameters of the VFT Temperature Dependence of the α_2 and α Processes and Mobility of Simultaneously Conducting Ions

	α_2 process		α process		conducting ion mobility			
sample	$\log(\omega_\infty)$ (rad/s)	D	$\log(\omega_\infty)$ (rad/s)	D	$\log(\mu_\infty)$ ($cm^2\ V^{-1}\ s^{-1}$)	D	T_0 (K)	DSC $T_g - T_0$ (K)
C_4-PF_6 (3a)	8.8	4.3	11.1	4.3	−1.0	3.7	217	39
C_4-Tf_2N (3b)	8.7	4.1	11.3	4.1	−1.1	3.4	196	34
C_{12}-PF_6 (3c)	9.2	5.6	11.0	5.6	−0.8	5.0	207	37
C_{12}-Tf_2N (3d)	8.8	5.0	10.8	5.0	−0.8	4.5	189	37

dipolar relaxations,[48,49] assigned to the usual segmental motion of the polymer (α) and a lower frequency relaxation that increases in strength with ion content,[49] (α_2) attributed to ions rearranging, for instance, exchanging states between isolated pairs and aggregates of pairs.

The peak relaxation frequencies of the α process of glass-forming liquids, polymers, and ionomers follow VFT temperature dependence with the same Vogel temperature T_0 as was found for the mobility of simultaneously conducting ions.

$$\omega_{max} = \omega_\infty \exp\left(-\frac{DT_0}{T - T_0}\right) \tag{14}$$

The curves in Figure 8a are fits to eq 14 using the T_0 from the mobility VFT fits in Figure 5 with strength parameter D and high-temperature limiting frequency ω_∞ listed in Table 4 for the α and α_2 processes. The α process involves segmental motion and hence is related to the glass transition. This is why PF_6^- ionomers having higher T_g exhibit slower α processes than Tf_2N^- ionomers having lower T_g. Many glass-forming liquids and nonionic polymers have ω_{max} of the α process ~0.01 rad/s at their T_g.[79] Here we extrapolate the VFT fits of the α process (eq 14 and curves in Figure 8a) to 0.01 rad/s to get the DRS T_g listed in Table 2. There is reasonable agreement between DRS T_g and DSC T_g for the ionomers with C_{12} tails but those with C_4 tails have DRS T_g ~ 8 K lower than DSC T_g and the DRS T_gs of the ionomers with the same anions (PF_6^- or Tf_2N^-) are nearly identical in spite of different tail length (also evident in Figure 8a). The ionomers with C_{12} tails aggregate most of their ions so the magnitude of the α_2 relaxation involving ion rearrangement is much smaller than for the ionomers with C_4 tails, and this is likely why there is a large difference in DRS and DSC T_gs of the ionomers with C_4 tails. Calorimetry sees both α and α_2 processes and is more impacted by the latter, slower process when its magnitude is stronger (see Supporting Information Figure S11).

In polymers with polar side groups, generally an α process is assigned to side-chain motion.[80] The observation that ionomers with n-butyl tails (**C_4-PF_6 (3a)** and **C_4-Tf_2N (3b)**) having higher T_g show even faster α process than those with n-dodecyl tails (**C_{12}-PF_6 (3c)** and **C_{12}-Tf_2N (3d)**) having lower T_g is connected to their fragility m, calculated by

$$m = -\left.\frac{d\log(\omega)}{d(T_g/T)}\right|_{T=T_g} = \frac{DT_0}{T_g(\ln 10)(1 - T_0/T_g)^2} \tag{15}$$

wherein D and T_0 are VFT fitting parameters for ω_α (open symbols in Figure 8a). The estimated fragility m values of these imidazolium-based ionomers are given in Table 2 with error estimates based on the extrapolation of the VFT fit to T_g, discussed above. The 25% higher fragility of ionomers with C_4 tails can be understood by the enhanced aggregation of the ionomers with C_{12} tails, reflected in the X-ray data of Figure 1. Aggregated ions present a strong energetic barrier for segmental motion that always lowers fragility.[81,82] Similar reductions in fragility with increasing side chain length have been reported for poly(n-alkyl methacrylates)[83] and poly(α-olefins).[84]

The peak relaxation frequencies of the α_2 processes of these ionomers occurring at frequencies ~2 orders of magnitude lower than those of the α processes also follow a VFT temperature dependence. Like the α process, Tf_2N^- ionomers have faster α_2 process than PF_6^- ionomers due to Tf_2N^- counterion imparting lower T_g. Ionomers with the same counterion have almost identical α_2 relaxation frequencies in spite of having different tail length. This suggests that the α_2 processes must be primarily related to rearrangements of ions that are not strongly aggregated, consistent with literature on dielectric spectroscopy of other single-ion conducting ionomers.[48,49,59] In Figure 8b, the relaxation strength $\Delta\varepsilon$ for the α_2 process is much larger than that for the α process. Additionally, $\Delta\varepsilon_{\alpha_2}$ has a strong temperature dependence, but $\Delta\varepsilon_\alpha$ has no temperature dependence with $\Delta\varepsilon_\alpha \approx 8$ for all four ionomers. The stronger α_2 process involving ionic rearrangements primarily determines the temperature dependence of ε_s shown in Figure 6. Interestingly, ionomers with n-butyl tails (**C_4-PF_6 (3a)** and **C_4-Tf_2N (3b)**) have much larger $\Delta\varepsilon_{\alpha_2}$ than those with n-dodecyl tails (**C_{12}-PF_6 (3c)** and **C_{12}-Tf_2N (3d)**), consistent with n-dodecyl tails promoting ion aggregation as seen in X-ray (Figure 1). The n-butyl tails in **C_4-PF_6 (3a)** and **C_4-Tf_2N (3b)** allow more ions to participate in conduction (Figure 4) and rearrange in the α_2 process, by not having so many aggregated ions.

H. Temperature Dependence of Ion Conduction and Polymer Relaxation. Conductivity is the product of charge e, number density of carriers p, and their mobility μ for single-ion conductors, so the temperature dependence of $\sigma_{DC}(T)$ shown in Figure 2 has already been evaluated by our Arrhenius fit of $p(T) = p_\infty \exp[-E_a/(RT)]$ in Figure 4 and our VFT fit of extended mobility $\mu(T) = \sigma_{DC}(T)/[\exp(T)]$ to eq 7 in Figure 5.

$$\sigma_{DC} = e\mu_\infty p_\infty \exp\left(-\frac{DT_0}{T - T_0}\right)\exp\left(-\frac{E_a}{RT}\right) \tag{16}$$

Predictions of eq 16 with parameters listed in Tables 3 and 4 are shown as the solid and dashed curves in Figure 2. The fact that ω_α, $\omega_{\alpha 2}$, μ, and σ_{DC} all share a common Vogel temperature demonstrates strong coupling between motion of counterions and polymer segmental dynamics. The Vogel temperature T_0 lies 37 K below the DSC glass transition temperature for each ionomer ($T_g - T_0 \approx 37$ K). A vital point is that the VFT fit in Figure 5 to extended mobility data calculated from conductivity enables this conclusion because conductivity is measured with high precision very close to T_g. Independent VFT fits to the

significantly less precise ω_α or $\omega_{\alpha 2}$ would *not* yield identical T_0 to that from extended mobility, but the Vogel temperature from extended mobility can give a good description of the temperature dependences of ω_α and $\omega_{\alpha 2}$ (compare curves and data in Figure 8a).

Barton, Nakajima, and Namikawa[85−87] (BNN) suggested that conduction and dielectric relaxation have their origins in one diffusion process and proposed a simple empirical scaling correlation between ionic conductivity σ_{DC} and the product of relaxation strength $\Delta\varepsilon$ and frequency at the loss maximum ω_{max}.

$$\sigma_{DC} \propto \Delta\varepsilon\omega_{max} \quad (17)$$

As shown in Figure 9, the conductivity can be successfully scaled in accordance with eq 17, further demonstrating that conductivity is strongly coupled with both ion motion (α_2 process) and polymer segmental motion (α process).

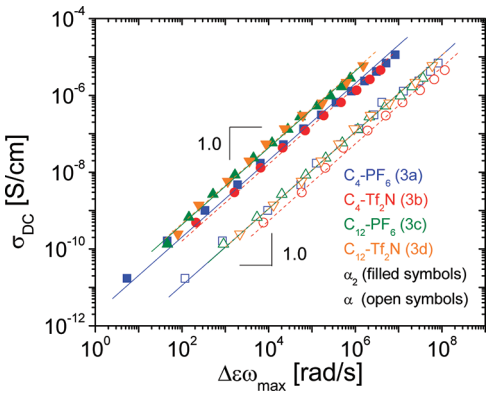

Figure 9. DC conductivity σ_{DC} against the product of relaxation strength $\Delta\varepsilon$ and frequency ω_{max} of the α_2 (filled symbols) and α (open symbols) processes. The solid and dashed lines are fits of the BNN law (eq 17) with slopes of unity.

4. CONCLUSIONS

This paper correlates morphology, ion conduction, and dielectric response of imidazolium-based single-ion conductors with two different anions and with two different imidazolium tail lengths. The effect of counterions is clearly observed in the glass transition temperature and ionic conductivity; Tf_2N^- ionomers with lower T_gs have higher ionic conductivities than PF_6^- ionomers with higher T_gs, as anticipated by *ab initio* calculations that show that the imidazolium cation is less prone to aggregation with Tf_2N^- counterions than with PF_6^- counterions. The ionic conductivity is also strongly coupled with ion motion (α_2) and polymer segmental motion (α) from the observation of a common Vogel temperature in the VFT temperature dependence of the mobility of simultaneously conducting ions μ, ion rearrangements (α_2), and polymer segmental motion (α).

The *n*-dodecyl tail results in strong ion aggregation over the whole temperature range studied, as clearly seen in X-ray scattering and dielectric constant. The *n*-butyl tail promotes very little ionic aggregation, with a significantly larger dielectric constant that agrees reasonably with the Onsager prediction. Significant increase of the relaxation strength of the ion rearrangement α_2 for ionomers with *n*-butyl tails accounts for the significantly larger static dielectric constants and higher mobilities for the simultaneously conducting ions.

■ ASSOCIATED CONTENT

Supporting Information

NMR and high resolution mass spectral data of 1-dodecylimidazole, **1a−d**, **2a−d**, and **4**; ^{1}H NMR spectra of **1a−d**, **2a−d**, **3b**, and **4**; DSC thermograms of **3a−d**; frequency dependence of loss tangent for **3a−d**. This material is available free of charge via the Internet at http://pubs.acs.org.

■ AUTHOR INFORMATION

Corresponding Author

*E-mail: rhc@plmsc.psu.edu.

Notes

The authors declare no competing financial interest.

■ ACKNOWLEDGMENTS

This work was supported in part by the U.S. Army Research Office under Grant W911NF-07-1-0452 Ionic Liquids in Electro-Active Devices (ILEAD) MURI. The authors are grateful to James McGrath and Timothy Long for use of their thermal analysis equipment, James Runt for use of his dielectric spectrometer, Terry L. Price Jr. for his help in analytical data collection, David Salas de la Cruz for his help in X-ray data collection, and Yossef Elabd, Friedrich Kremer, James Runt, and Qiming Zhang for many helpful discussions.

■ REFERENCES

(1) *Ab initio* calculations exhibit that the ion dissociation energy at 0 K for 1-buty-3-methylimidazolium cation with Tf_2N^- counterion (310 kJ/mol) is much lower than that for lithium cation with Tf_2N^- counterion (580 kJ/mol).

(2) Welton, T. *Chem. Rev.* **1999**, *99*, 2071.

(3) Buzzeo, M. C.; Evans, R. G.; Compton, R. G. *ChemPhysChem* **2004**, *5*, 1106.

(4) Ohno, H. *Electrochemical Aspects of Ionic Liquids*; Wiley-Interscience: Hoboken, NJ, 2005.

(5) Hapiot, P.; Lagrost, C. *Chem. Rev.* **2008**, *108*, 2238.

(6) Weingärtner, H. *Angew. Chem., Int. Ed.* **2008**, *47*, 654.

(7) Soukup-Hein, R. J.; Warnke, M. M.; Armstrong, D. W. *Annu. Rev. Anal. Chem.* **2009**, *2*, 145.

(8) Armand, M.; Endres, F.; MacFarlane, D. R.; Ohno, H.; Scrosati, B. *Nat. Mater.* **2009**, *8*, 621.

(9) Green, M. D.; Long, T. E. *Polym. Rev.* **2009**, *49*, 291.

(10) Leys, J.; Wübbenhorst, M.; Menon, C. P.; Rajesh, R.; Thoen, J.; Glorieux, C.; Nockemann, P.; Thijs, B.; Binnemans, K.; Longuemart, S. *J. Chem. Phys.* **2008**, *128*, 064509.

(11) Huddleston, J. G.; Visser, A. E.; Reichert, W. M.; Willauer, H. D.; Broker, G. A.; Rogers, R. D. *Green Chem.* **2001**, *3*, 156.

(12) Nanjundiah, C.; McDevitt, S. F.; Koch, V. R. *J. Electrochem. Soc.* **1997**, *144*, 3392.

(13) Doyle, M.; Choi, S. K.; Proulx, G. *J. Electrochem. Soc.* **2000**, *147*, 34.

(14) Lu, W.; Fadeev, A. G.; Qi, B. H.; Smela, E.; Mattes, B. R.; Ding, J.; Spinks, G. M.; Mazurkiewicz, J.; Zhou, D. Z.; Wallace, G. G.; MacFarlane, D. R.; Forsyth, S. A.; Forsyth, M. *Science* **2002**, *297*, 983.

(15) Ue, M.; Takeda, M.; Toriumi, A.; Kominato, A.; Hagiwara, R.; Ito, Y. *J. Electrochem. Soc.* **2003**, *150*, A499.

(16) Sakaebe, H.; Matsumoto, H. *Electrochem. Commun.* **2003**, *5*, 594.

(17) Xu, W.; Angell, C. A. *Science* **2003**, *302*, 422.

(18) Fernicola, A.; Scrosati, B.; Ohno, H. *Ionics* **2006**, *12*, 95.

(19) Galinski, M.; Lewandowski, A.; Stepniak, I. *Electrochim. Acta* **2006**, *51*, 5567.

(20) Zhu, Q.; Song, Y.; Zhu, X.; Wang, X. *J. Electroanal. Chem.* **2007**, *601*, 229.

(21) Greaves, T. L.; Drummond, C. J. *Chem. Rev.* **2008**, *108*, 206.

(22) Ohno, H.; Ito, K. *Chem. Lett.* **1998**, 751.

(23) Yoshizawa, M.; Ohno, H. *Chem. Lett.* **1999**, 889.

(24) Snedden, P.; Cooper, A. I.; Scott, K.; Winterton, N. *Macromolecules* **2003**, *36*, 4549.
(25) Ohno, H.; Yoshizawa, M.; Ogihara, W. *Electrochim. Acta* **2004**, *50*, 255.
(26) Washiro, S.; Yoshizawa, M.; Nakajima, H.; Ohno, H. *Polymer* **2004**, *45*, 1577.
(27) Nakajima, H.; Ohno, H. *Polymer* **2005**, *46*, 11499.
(28) Ogihara, W.; Suzuki, N.; Nakamura, N.; Ohno, H. *Polym. J.* **2006**, *38*, 117.
(29) Ogihara, W.; Washiro, S.; Nakajima, H.; Ohno, H. *Electrochim. Acta* **2006**, *51*, 2614.
(30) Ohno, H. *Macromol. Symp.* **2007**, *249*, 551.
(31) Green, O.; Grubjesic, S.; Lee, S.; Firestone, M. A. *Polym. Rev.* **2009**, *49*, 339.
(32) Xie, M.; Han, H.; Ding, L.; Shi, J. *Polym. Rev.* **2009**, *49*, 315.
(33) Chen, H.; Choi, J. H.; Salas-de La Cruz, D.; Winey, K. I.; Elabd, Y. A. *Macromolecules* **2009**, *42*, 4809.
(34) Lee, M.; Choi, U. H.; Colby, R. H.; Gibson, H. W. *Chem. Mater.* **2010**, *22*, 5814.
(35) Wang, Y.; Voth, G. A. *J. Am. Chem. Soc.* **2005**, *127*, 12192.
(36) Wang, Y.; Voth, G. A. *J. Phys. Chem. B* **2006**, *110*, 18601.
(37) Jiang, W.; Wang, Y.; Yan, T.; Voth, G. A. *J. Phys. Chem. C* **2008**, *112*, 1132.
(38) Lopes, J. N. A. C.; Padua, A. A. H. *J. Phys. Chem. B* **2006**, *110*, 3330.
(39) Margulis, C. J. *Mol. Phys.* **2004**, *102*, 829.
(40) Delsignore, M.; Maaser, H. E.; Petrucci, S. *J. Phys. Chem.* **1984**, *88*, 2405.
(41) Sun, X. G.; Kerr, J. B.; Reeder, C. L.; Liu, G.; Han, Y. *Macromolecules* **2004**, *37*, 5133.
(42) Bottcher, C. J. F. *Theory of Electric Polarization*; Elsevier: Amsterdam, 1973; Vol. *1*.
(43) Kremer, F.; Schonhals, A. *Broadband Dielectric Spectroscopy*; Springer-Verlag: New York, 2002.
(44) Macdonald, J. R. *Phys. Rev.* **1953**, *92*, 4.
(45) Coelho, R. *Rev. Phys. Appl.* **1983**, *18*, 137.
(46) Barsoukov, E.; Macdonald, J. R. *Impedance Spectroscopy Theory, Experiment and Applications*; Wiley: New York, 2005.
(47) Klein, R. J.; Zhang, S.; Dou, S.; Jones, B. H.; Colby, R. H.; Runt, J. *J. Chem. Phys.* **2006**, *124*, 144903.
(48) Fragiadakis, D.; Dou, S.; Colby, R. H.; Runt, J. *Macromolecules* **2008**, *41*, 5723.
(49) Fragiadakis, D.; Dou, S.; Colby, R. H.; Runt, J. *J. Chem. Phys.* **2009**, *130*, 064907.
(50) Becke, A. D. *J. Chem. Phys.* **1993**, *98*, 5648.
(51) Lee, C.; Yang, W.; Parr, R. G. *Phys. Rev. B* **1988**, *37*, 785.
(52) Stephens, P. J.; Devlin, F. J.; Chabalowski, C. F.; Frisch, M. J. *J. Phys. Chem.* **1994**, *98*, 11623.
(53) Heiney, P. A. *Comm. Powder Diffr. Newsl.* **2005**, *32*, 9.
(54) Beilstein test: A copper wire was heated in a burner flame until there was no further coloration of the flame. The wire was allowed to cool slightly, then dipped into the monomer, and again heated in the flame. A green flash is indicative of halide ions, whereas pure Tf_2N^- and PF_6^- salts give orange or red colors.
(55) van Krevelen, D. W. *Properties of Polymers*; Elsevier: New York, 1990.
(56) Annapureddy, H. V. R.; Kashyap, H. K.; De Biase, P. M.; Margulis, C. J. *J. Phys. Chem. B* **2010**, *114*, 16838.
(57) Salas-de la Cruz, D.; Green, M. D.; Ye, Y. S.; Elabd, Y. A.; Long, T. E.; Winey, K. I. *J. Polym. Sci., Part B: Polym. Phys.* **2012**, *50*, 338.
(58) Wang, W.; Liu, W. J.; Tudryn, G. J.; Colby, R. H.; Winey, K. I. *Macromolecules* **2010**, *43*, 4223.
(59) Wang, W.; Tudryn, G. J.; Colby, R. H.; Winey, K. I. *J. Am. Chem. Soc.* **2011**, *133*, 10826.
(60) Russina, O.; Triolo, A.; Gontrani, L.; Caminiti, R.; Xiao, D.; Hines, L. G.; Bartsch, R. A.; Quitevis, E. L.; Pleckhova, N.; Seddon, K. R. *J. Phys.: Condens. Matter* **2009**, *21*, 424121.
(61) Bhargava, B. L.; Devane, R.; Klein, M. L.; Balasubramanian, S. *Soft Matter* **2007**, *3*, 1395.
(62) Coelho, R. *J. Non-Cryst. Solids* **1991**, *131*, 1136.
(63) Coelho, R. *Physics of Dielectrics for the Engineer*; Elsevier: New York, 1979.
(64) Tudryn, G. J.; Liu, W. J.; Wang, S. W.; Colby, R. H. *Macromolecules* **2011**, *44*, 3572.
(65) Wang, S. W.; Liu, W. J.; Colby, R. H. *Chem. Mater.* **2011**, *23*, 1862.
(66) Tokuda, H.; Hayamizu, K.; Ishii, K.; Susan, M. A. B. H.; Watanabe, M. *J. Phys. Chem. B* **2005**, *109*, 6103.
(67) Onsager, L. *J. Am. Chem. Soc.* **1936**, *58*, 1486.
(68) Hill, N. E.; Vaughan, W. E.; Price, A. H.; Davies, M. *Dielectric Properties and Molecular Behaviour*; Van Nostrand Reinhold Co.: London, 1969.
(69) Fröhlich, H. *Theory of Dielectrics: Dielectric Constant and Dielectric Loss*; Clarendon Press: London, 1949.
(70) Kirkwood, J. G. *J. Chem. Phys.* **1939**, *7*, 911.
(71) Oster, G.; Kirkwood, J. G. *J. Chem. Phys.* **1943**, *11*, 175.
(72) Izgorodina, E. I.; Forsyth, M.; MacFarlane, D. R. *Phys. Chem. Chem. Phys.* **2009**, *11*, 2452.
(73) Wübbenhorst, M.; van Turnhout, J. *J. Non-Cryst. Solids* **2002**, *305*, 40.
(74) Boersma, A.; van Turnhout, J.; Wübbenhorst, M. *Macromolecules* **1998**, *31*, 7453.
(75) Diaz-Calleja, R. *Macromolecules* **2000**, *33*, 8924.
(76) The actual EP is often slightly broader than Debye, and in the past we have fit EP to an asymmetric broader function[49] and to a symmetric Cole−Cole function.[65] These yield results for EP that are qualitatively identical and nearly quantitatively identical to those from Debye fitting, which is far simpler. When the asymmetric function is used with slopes of 1.91 for Tf_2N^- ionomers and 1.88 for PF_6^- ionomers on the high frequency side of EP, the conducting ion content p is increased 2.1-fold (Tf_2N^-) and 1.7-fold (PF_6^-) at all temperatures where tan δ shows a maximum for EP and the activation energy E_a was identical.
(77) Daguenet, C.; Dyson, P. J.; Krossing, I.; Oleinikova, A.; Slattery, J.; Wakai, C.; Weingärtner, H. *J. Phys. Chem. B* **2006**, *110*, 12682.
(78) Nakamura, K.; Shikata, T. *ChemPhysChem* **2010**, *11*, 285.
(79) Angell, C. A. *Chem. Rev.* **1990**, *90*, 523.
(80) Yamane, M.; Hirose, Y.; Adachi, K. *Macromolecules* **2005**, *38*, 10686.
(81) Adam, G.; Gibbs, J. H. *J. Chem. Phys.* **1965**, *43*, 139.
(82) Rodenburg, B. V.; Sidebottom, D. L. *J. Chem. Phys.* **2006**, *125*, 024502.
(83) Floudas, G.; Stepanek, P. *Macromolecules* **1998**, *31*, 6951.
(84) Stukalin, E. B.; Douglas, J. F.; Freed, K. F. *J. Chem. Phys.* **2009**, *131*, 114905.
(85) Namikawa, H. *J. Non-Cryst. Solids* **1974**, *14*, 88.
(86) Namikawa, H. *J. Non-Cryst. Solids* **1975**, *18*, 173.
(87) Dyre, J. C. *Phys. Rev. B* **1993**, *48*, 12511.